DESY PRC 00-02

Letter of Intent to Upgrade the Longitudinal Polarimeter

E.Barrelet[1],V.Brisson[2], M.Jacquet-Lemire[2], A. Reboux[2], C. Pascaud[2], F. Zomer[2]
and the POL2000 group[3]

[1]IN2P3-CNRS

[2]Laboratoire de l'accélérateur Linéaire, IN2P3-CNRS et Université de Paris-Sud

B.P. 34 - F-91898 ORSAY CEDEX, France

[3]members from DESY, HERMES, H1 and Zeus*

April 27, 2000

Abstract

We propose to construct a new laser system to significantly increase the power of the existing longitudinal polarimeter. The main ingredient of the new system is a Fabry-Perot cavity around the laser-electron beam interaction point, which allows to reach very large laser power at the interaction point, resulting in significantly larger backscattered Compton photon rates.

*See DESY PRC-99-01 for a detailed list of members of this group. Contact Ties.Behnke@desy.de

1 Introduction

After the luminosity upgrade physics with polarized lepton beams will be an integral part of the HERA physics program for the three experiments which are utilizing the lepton beam (HERMES, H1 and ZEUS). While HERMES has been doing physics with polarized beams for a long time, H1 and Zeus will only be able to do so after the installation of spin rotators during the 2000 shutdown.

Polarized leptons will give access to the helicity structure of the weak current in e-p collisions. This allows precision measurements of the coupling constants of the weak current within the standard model, and to search for deviations from the standard model by e.g. looking for right handed charged currents.

HERA with polarized leptons will have a unique potential which complements the existing and expected data from LEP and other colliders. To fully exploit this potential a high lepton beam polarization and a precise determination of the polarization are important.

The structure of this paper is as follows. After a brief review of the existing polarimeter system we present the proposed upgrade to the longitudinal polarimeter. This is followed by a presentation of the main technical parameters and the proposed implementation. At the end of the paper a number of rather detailed appendices are included, where details about some of the calculations done to prove the feasibility of the device at HERA are shown.

1.1 The existing polarimeter system at HERA

Currently the measurement of the electron polarization at HERA is done with two different devices. A program for a modest upgrade of the system to cope with the larger demands on the polarization precision after the upgrade has been presented previously [1]. The transverse polarimeter (TPOL) [2] which is located in the West area of HERA measures the polarization of the – at that location – transversely polarized beam. The longitudinal polarimeter (LPOL) [3] in contrast measures the longitudinal polarization of the beam near the HERMES interaction point.

Both devices measure the polarization through the scattering of laser light off the lepton beam, and detecting the backscattered photons.

Up to now the TPOL is calibrated in an "experimental" fashion through rise-time curves. The rise of the polarization in the machine is related to the asymptotic polarization by theoretical considerations. If the machine is "flat" (no spin rotators are switched on), and if beams are not colliding, these calibrations can be done with good precision. They were done most recently in 1994, and these calibration are still used today. They dominate the systematic error of the TPOL with a contribution of 3.5%.

Recent studies have resulted in a much better modeling of the detector and the energy distributions measured as a function of the polarization. This together with an improved description of the spatial calibration of the device will allow a re-calibration of the TPOL. We are confident that the systematic errors can be reduced to the level of $\Delta\mathcal{P}/\mathcal{P} \approx 1\%$ already in the very near future. Further enhancements of the analysis and the data quality might result in further reductions of the error.

The LPOL is at the moment operated in the multi-photon mode. The final error of the polarization measured with this device depends critically on the calibration of the linearity of the energy scale of the calorimeter. This was done in a test beam at CERN, where a significantly non-linear response of the device was found. The deviation is as large as 15% at large energies. Compared to a perfectly linear detector, this changes the analyzing power of the calorimeter from 18% to 19.3%.

Nevertheless a careful analysis of the current data and system leads to an error of the polarization of $\Delta\mathcal{P} = 0.010/\mathrm{min}$ statistical for groups of bunches, and $\Delta\mathcal{P} = 0.009$ systematical. The dominant contribution to the systematic error comes from the knowledge of the calibration of the calorimeter.

A powerful indicator of the quality of the data from both devices is the ratio of both polarizations. This ratio has been studied in detail for the 1999 data. After some quality cuts, around 80% of all data survive and are used in the analysis. Plotting the error against the integration time, an asymptotic systematic error of $\Delta(\mathcal{P}_{\mathrm{LPOL}}/\mathcal{P}_{\mathrm{TPOL}}) = 0.016$ is found. If harder quality cuts are applied (in particular, only runs with a polarization $\mathcal{P} > 0.5$ are used), the error is reduced to around 0.01. This error is fairly well compatible with the ones quoted above, which indicates that the contribution from correlated errors is fairly small. However such a method can never detect changes in the overall scale of the polarization, if both devices are affected in the same way. Therefore independent and powerful calibration methods are needed for each polarimeter itself.

The current performance of the polarimeters is summarized in table 1.

	TPOL		LPOL	
	all bunches	per bunch	all bunches	per bunch
t for $\sigma = 1\%$	1 min	-	2 min	>30 min
$\sigma_{\mathrm{sys}}/\mathcal{P}$	3.6%	-	1.8%	1.8%
dominant σ_{sys}	$\eta - y$		CALO	

$\eta - y$: $\eta - y$ transformation function of the TPOL calorimeter
IP: Interaction point between the laser and the lepton beam
CALO: Calibration of the calorimeter for the LPOL, mostly linearity

Table 1: Comparative table of the performance of the two polarimeters TPOL and LPOL. The time given in the first line are the time it takes to measure the polarization with a statistical error of $\sigma_{\mathcal{P}}/\mathcal{P} = 1\%$, either for all bunches (left column), or for single bunches (right column) and a total lepton-beam current of around 20 mA. In the last row the at the moment dominant systematic error is listed. New analysis techniques or improved understanding of the detector might of course change the picture.

1.2 The Physics Case for Polarization

In this section we will concentrate on the physics program of the colliding beam experiments, since the relevant arguments for HERMES were presented in an earlier proposal for the original installation of the longitudinal polarimeter [4]. The detailed physics motivation has been presented in a number of documents [5, 6, 7], and will not be repeated here. Instead we will concentrate on the arguments, which support both a fast and high precision determination of the polarization.

One of the main objectives of the HERA physics program after the upgrade will be the measurement of the deep inelastic cross section at high Q^2 using polarized electron and positron beams.

The cross sections for the neutral current in ep collisions with a polarized lepton beam is written as:

$$\sigma_{NC}^{e^{\pm}p} = \frac{2\pi\alpha^2}{xQ^4}\left(H_0^{\pm} + PH_P^{\pm}\right)$$

$$\mathrm{H}_{0,P}^{\pm} = \left(1+(1-y)^2\right)\ F_2^{0,P} \mp \left(1-(1-y)^2\right)\ xF_3^{0,P}.$$

Here P denotes the lepton beam polarization and is defined by:

$$\mathcal{P} = (N_R - N_L)/(N_R + N_L)$$

N_R and N_L are the number of right-handed and left-handed leptons in the beam respectively. For large Q^2, where the longitudinal function F_L can be neglected, $F_2^{0,\mathcal{P}}$ and $xF_3^{0,\mathcal{P}}$ are the DIS structure functions and contain linear combination of the quark densities and quadratic functions of the vectorial and axial couplings of the fermions to the Z^0.

The cross sections for charged current processes are written as:

$$\sigma_{CC}^{e^+p} = (1+\mathcal{P})\,\frac{G_\mu^2}{2\pi}\left(\frac{M_W^2}{Q^2+M_W^2}\right)^2\ \left(\bar{u}+\bar{c}+(1-y)^2(d+s+b)\right)$$

$$\sigma_{CC}^{e^-p} = (1-P)\,\frac{G_\mu^2}{2\pi}\left(\frac{M_W^2}{Q^2+M_W^2}\right)^2\ \left(u+c+(1-y)^2(\bar{d}+\bar{s}+\bar{b})\right)$$

1.2.1 Vector and axial couplings

From the study of the NC events for different lepton charges and polarizations, the vector- and axial-coupling constants v_u, v_d, a_u and a_d can be measured. With an integrated luminosity of 1000pb^{-1} and a polarization P$\sim$ 60 - 70%, an accuracy comparable to the one obtained by LEP for the couplings of the heavy quarks b and c can be obtained [5]. The coupling constants a_u and a_d can be measured with unpolarized beam, but the polarization gives an increased sensitivity. Polarized beams are necessary for determining the vector couplings v_u and v_d.

The charged current cross section is directly proportional to $(1 \pm \mathcal{P})$. Thus a high level of polarization translates directly into an effective increase of the statistics. However the increase of the statistics has to be matched by correspondingly small systematic errors. For example, if 250 pb^{-1} per charge and per polarization state of data are available the up-quark coupling to the Z-boson can be measured with a precision of 10%, if the polarization is known to 1%.

1.2.2 W mass measurement

Even though HERA cannot reconstruct on-mass shell W bosons, as is done e.g. at LEP or the Tevatron, indirect information on the properties of the W is accessible. In particular it will be possible to determine the mass of the W in the framework of the standard model to an accuracy of 55 MeV (which compares well to the precision of the LEP experiments) from 1000 pb^{-1} of data taken with a 70% polarized electron beam [7]. This scenario assumes a 1% relative systematic uncertainty on the measured cross sections (this accuracy decreases to $\delta M_W \sim 81$ MeV for a systematic error of 2%).

Assuming a luminosity L and a polarization P, the measured CC cross section is written as a function of the number of selected events (for a electron incident beam):

$$\sigma_{CC} = \frac{N^{evts}}{L(1-\mathcal{P})} \qquad (1)$$

The final error of the cross section will depend on the knowledge of the luminosity and the polarization individually for each bunch. Two effects have to be considered:

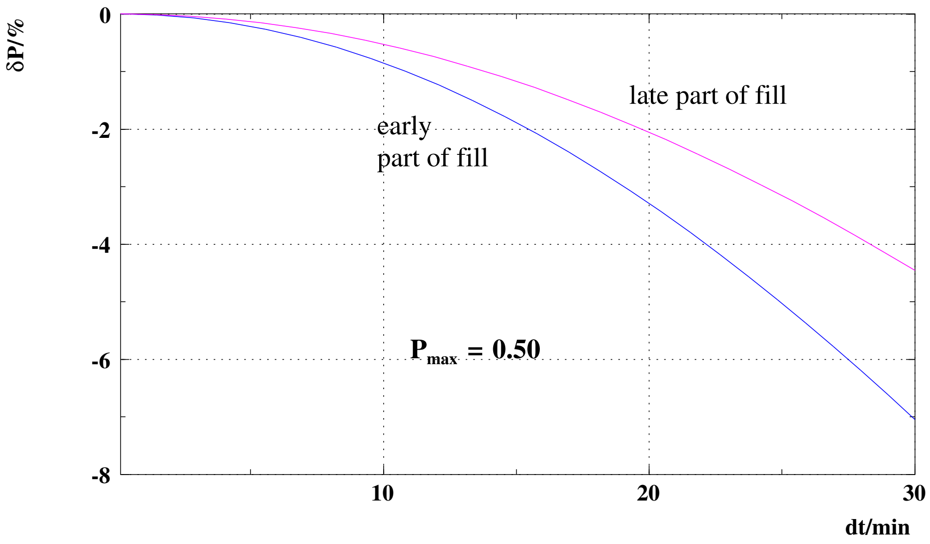

Figure 1: Systematic error (absolute error) incurred if the polarization is measured at fixed intervals during the early part of a fill (lower curve) and during the later part of a fill, as a function of the measurement interval.

- the precision with which the polarization can be measured

$$\left(\frac{d\sigma}{\sigma}\right)_{meas} \sim \left|\frac{\mathcal{P}}{1-\mathcal{P}}\right| \frac{d\mathcal{P}}{\mathcal{P}} \tag{2}$$

- possible variations of the polarization between bunches and as a function of time have to be tracked. This is of particular importance during the early stage of a fill, when the polarization is building up.

At the beginning of a fill after polarization has been established, but the lifetime of the electron beam is still small ($\sim 1.5\ h$), the typical time scale for a change of the polarization by ~ 1 % is ~ 10 min. Later in a fill the polarization stays essentially constant, except in exceptional circumstances, when a sudden loss of polarization may occur. During the early times of a fill however the luminosity is also the largest. It is during this time that the requirements for a fast polarization measurement are the most stringent. In addition for may measurements the luminosity weighted polarization is important. Differences in luminosity between individual bunches have been observed at the 15% level. No comparable high statistics data exist for the polarization, but the existing data are compatible with difference as large as 10%. These two numbers together with the requirement to make available reliable polarization data during the early part of a fill have led to the conclusion that the polarization should be measured for every bunch every few minutes at the 1% level. This is demonstrated in figure 1 [8].

1.2.3 Limit on $\sigma_{\mathbf{R}}$

An other very stringent limit for the precision with which the polarization has to be measured comes from the search of a non-vanishing right-handed current cross-section. Indeed, if one assumes that

$$\sigma_{CC}^{e^-p} = (1-\mathcal{P})\sigma_{SM} + (1+\mathcal{P})\sigma_R \tag{3}$$

a cross section measurement at two different values of the polarization should give an upper limit on σ_R. Depending on theoretical models, upper limits on σ_R can be converted to lower limits on the mass of a right-handed W_R boson. For instance, a cross section limit of

$\sigma_R/\sigma_{SM} < 2\%$ should lead to $M_{W_R} > 300$ GeV[6] (this lower limit is comparable to the one coming from $p\overline{p}$ experiments at Fermilab collider). This assumes that the total integrated luminosity was 500 pb^{-1} with a polarization of 70%, and that the data are shared equally between P and −P.

In order that the polarization error does not limit the measurement the total uncertainty from polarization should be below that of the cross section, say at 1% absolute. For 70% polarization this translates into a relative error on the polarization of 1.7%. If one factors the uncertainly from bunch by bunch into the equation, the polarization has to be measured at the level of $d\mathcal{P}/\mathcal{P} \sim 2.2\%$ per bunch.

1.2.4 Operation of HERA

A fast and high precision measurement of the polarization is not only important for the experiments, but also for the machine, since it allows a better and faster tuning of the collider for polarization. The polarization is optimized by changing a number of parameters in the HERA lepton ring. Since it is a complicated and coupled system, changing one parameter alone does not necessarily result in a clear reaction of the machine. Having a fast feedback on the actual polarization in the machine should ease the job for the operators of finding an optimal operating point in this complicated multi-parameter space.

2 The proposed new Longitudinal Polarimeter

The current system of polarimeters, after the already approved upgrades, will meet the requirements as defined in 1998 of a polarization measurement with a relative precision of $1 - 2\%$ for groups of bunches. However there are a few shortcomings in the current system:

- neither of the two systems delivers enough data to allow a high precision measurement of the polarization for individual bunches on a minute to minute base;
- neither of the two systems has a high enough statistical power to quickly follow small changes of the polarization in the machine;
- both system require external calibration input. This is particularly so for the multi-photon LPOL. Any high precision analysis of the polarization will be difficult to defend in the absence of online calibration data.

We therefore propose to upgrade the existing LPOL through the addition of a new laser system so that:

- a powerful enough laser is available so that the LPOL can be operated in the single photon mode;
- the statistical power is large enough for a measurement of the polarization of individual bunches within short (few minutes) times;
- enough data can be taken in the single photon mode that a full calibration of the calorimeter is possible without resorting to external inputs.

2.1 Overview of the proposed upgrade

We propose to add to the existing LPOL pulsed laser a system based on a CW laser and Fabry-Perot cavity around the interaction point of the laser beam with the lepton beam. In figure 2 the statistical error of the polarization is shown as a function of the probability of obtaining a scattered Compton photon. It is assumed that one measurement per minute

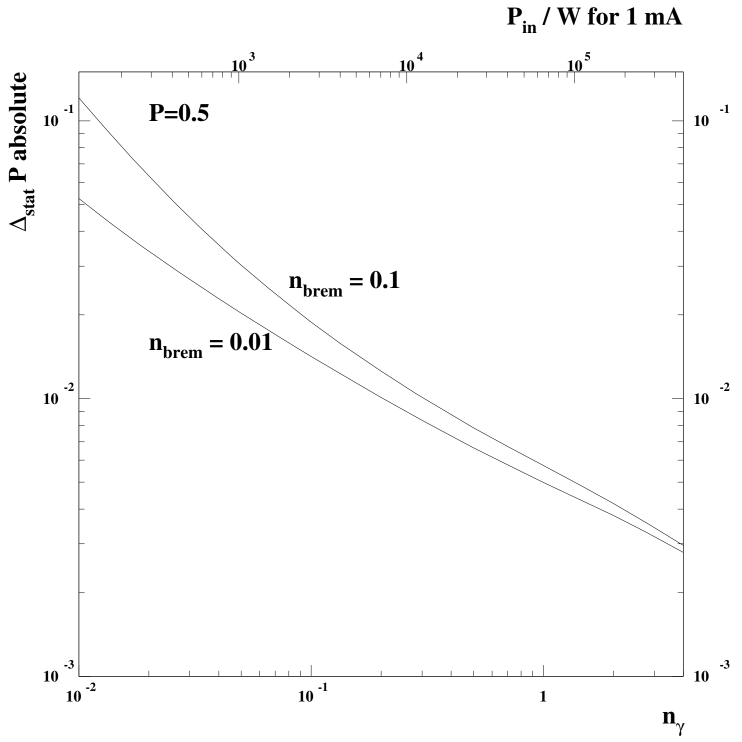

Figure 2: Statistical error of the polarization, as a function of the probability, n_γ, to obtain a backscattered photon, for 1% background and for 10% background. Also shown is the laser power needed to obtain the backscatter rate, assuming a crossing angle of 58 mrad.

is done, and that only one bunch in the machine is used. Also shown on the plot is the equivalent laser power needed. From this plot it is clear that a high laser power is needed, which cannot be easily obtained with commercial lasers. The required error can only be reached if the system is operated in the few photon mode, where on average one photon is backscattered into the detector bunch crossing [1].

The cavity will be installed next to the existing laser-lepton beam interaction point, so that any interference with the existing system is minimized. The whole system of laser and cavity will be installed on a self-contained table, so that no long laser transport lines are needed.

The backscattered Compton Photons will be detected in the photon detector from the current LPOL. A new dedicated fast data acqusition system will have to be added, in order to handle the expected higher rates.

In principle the addition of a detector to tag not only the backscattered photon but also the scattered electron would significantly enhance the capability of the device. This was

[1] Three different modes of operation can be distinguished for a polarimeter using the backscattered photon beam:

- Single Photon Mode: The probability to scatter a photon is very low, so that at most one photon is detected in the detector.
- Few Photon Mode: the probability is high enough that on average one photon per interaction is observed. In the detector a distribution ranging from one to a few photons is detected. The shape of the Compton spectra is still visible.
- Multi Photon Mode: Per interaction a large number of photons is scattered into the detector (e.g. around 1000 for the LPOL)

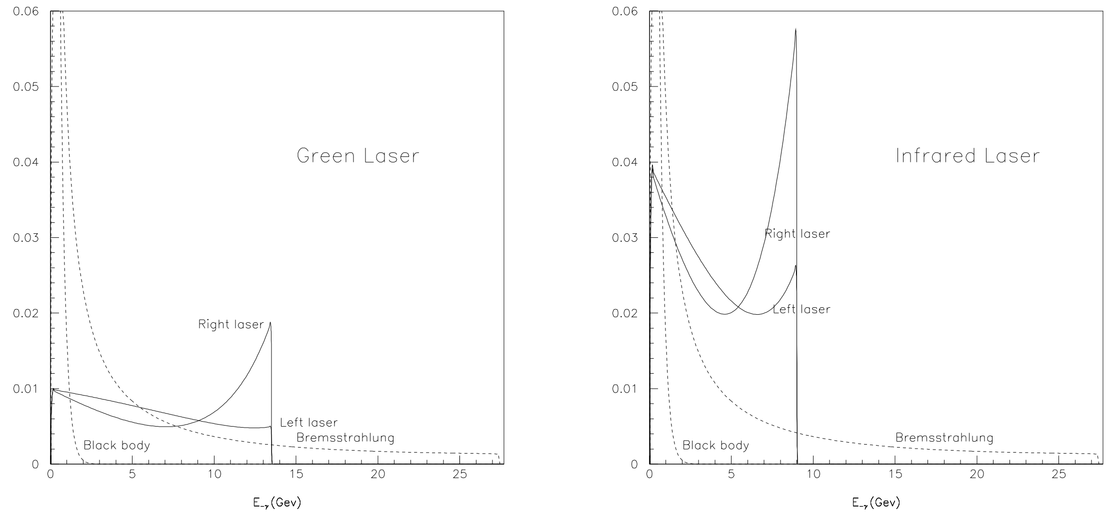

Figure 3: Compton backscattered energy spectra for a green laser (left figure) operating at 532 nm, and an infrared laser (1064 nm) (right figure). Shown are the signal spectra for left and right polarized light, and the dominant backgrounds from bremsstrahlung and black body radiation.

studied in the original LPOL proposal [4]. It was rejected because of the rather limited phase space for tagging the scattered electron. We propose to investigate this option also, though at a lower priority than the laser cavity.

2.2 Estimated Performance of the upgraded Polarimeter

The energy spectra for single photons which will be observed in the calorimeter are shown in figure 3 for left- and right-polarized photons. Superimposed are also the two main sources of background:

- bremsstrahlung photons, which are produced by the electron beam hitting the residual gas in the vacuum pipe.
- blackbody photons, produced by collisions between the electrons / positrons and photons emitted from the 310K hot beampipe walls.

For the analysis is was assumed that synchrotron photons are essentially eliminated through a filter in front of the calorimeter, as is done with the current device.

The data have been simulated in a parametric Monte Carlo. The simulation includes:

- the superposition of any number of backscattered Compton γ, beam-gas Bremsstrahlung photons, and blackbody photons;
- Gaussian smearing of the detector energy response and pedestal effects;
- a model for the dead material in front of the calorimeter (thanks to G. Grindhammer).

The three distributions: Laser-left, Laser-right, Laser-off are fitted simultaneously. The free parameters are the average number of bremsstrahlungs-, blackbody-, and laser-photons and the electron polarization.

The method has been checked with existing data from the LPOL. In figure 4 two example spectra as recorded by the LPOL are shown, with the result of the fit superimposed. The two spectra cover the range of true single photon operation to few photon operation. The background is found to be below 10%. The fits describe the shape of the spectra very well.

From the simulation it is concluded that it is possible to extract the polarization with an error of less than one percent, even in the presence of significant backgrounds.

2.3 Calibration of the LPOL

A strength of the LPOL operated in the few photon mode is that it allows a complete calibration of the device through data, thus eliminating the need to extrapolate test beam calibration data to real data taking conditions. The quality of the calibration has been investigated in the simulation based on the assumption that the device is operated in the few photon mode. In figure 5 a spectrum is shown as simulated for a Compton scattering rate of around 1 γ per bunch crossing. Note that the shape of the spectra, while from the simulation, has been checked with real data taken with the current LPOL operating in this mode. The Compton edges for one, two and three photons are clearly visible in the plot. They can be extracted from the data, and provide an in-situ calibration of the energy response and linearity of the device. From the simulation, it should be possible to reconstruct the different peak positions to better than 0.1%, which translates into a systematic error of the polarization of well below 0.1%.

Another fix-point for the calibration is given by the point where the energy weighted asymmetry crosses zero. This method is best suited to a system operating in the single photon mode. To cross check the calibration, data can be taken with the device with an attenuated laser, recording true single photon spectra. These data could then be used to provide another independent energy calibration point.

In conclusion we are convinced that a longitudinal polarimeter operated in this mode can be calibrated in-situ to an accuracy of better than one percent.

3 Technical Description of the new LPOL

A high laser power is required to operate the LPOL in the few photon mode. We propose to use a Fabry-Perot cavity[2] to reach the needed energy densities at the interaction point. Such a device is already operating successfully at CEBAF (Jefferson Lab) [9], under conditions which are very similar to those at HERA.

3.1 Description of the overall System

The proposed system is shown in figure 6. It consists of a small 0.7 W laser, which is mounted on an optical table close to the electron beam line. The laser light is sent through a Pockels-cell which defines the laser light polarization, and is then reflected into the cavity. The cavity is a monolithic cavity mounted around the beam pipe, intersecting the electron beam at an angle of 3.3 degree. The whole setup is mounted on an optical table. The cavity and beampipe are coupled to the HERA beampipe through bellows, to eliminate the transmission of vibrations into the optical system. It is put inside a small hut whose temperature is controlled. To ensure a phase lock between the cavity and the laser, a commercially available tunable laser is employed. This allows us to build the cavity as a monolithic device, with no active elements on the cavity itself.

[2]This device was originally proposed by P.Hello from the VIRGO collaboration.

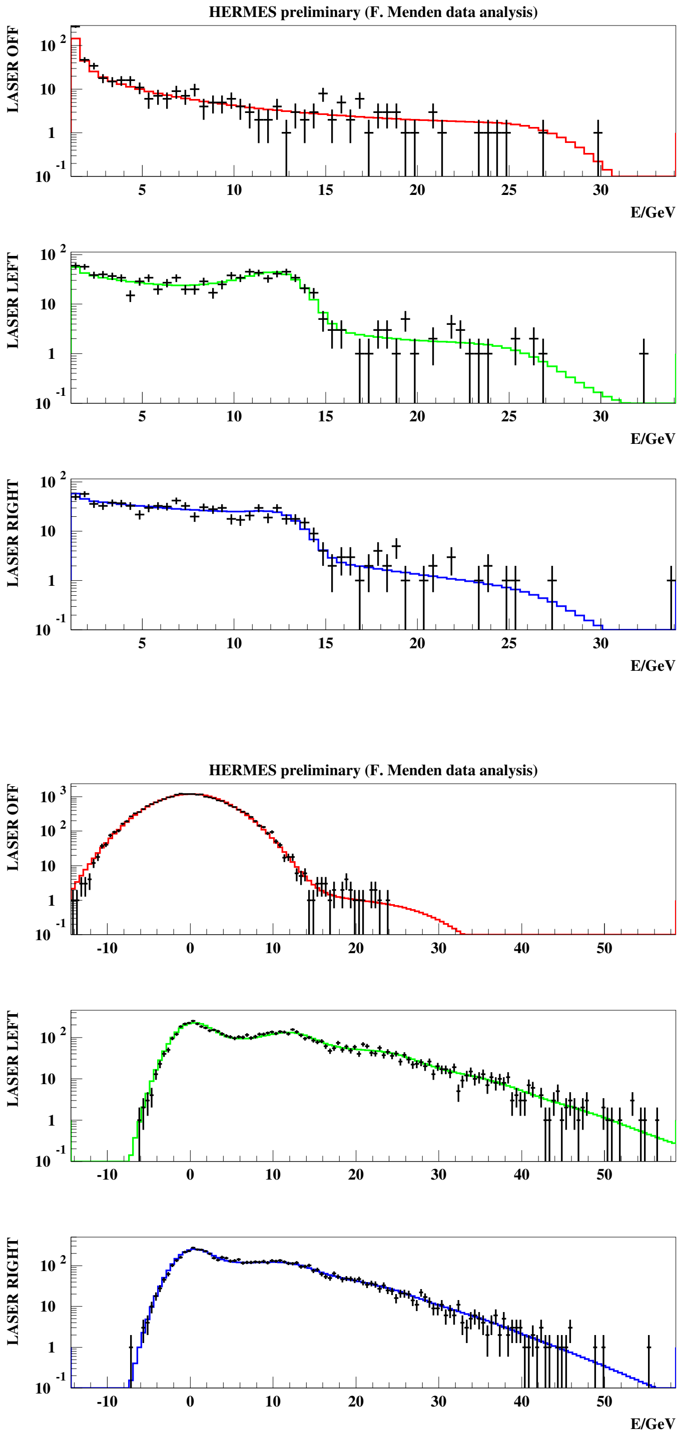

Figure 4: Fits to data taken with the LPOL in 1999. Top plots: The LPOL laser was attenuated to operate in the single photon mode: $n_\gamma \approx 0.22$ ($P_e \approx 60\%$) Bottom plots: The intensity of the laser was tuned to correspond to the few-photon mode: $n_\gamma \approx 1.5$ ($P_e \approx 60\%$)

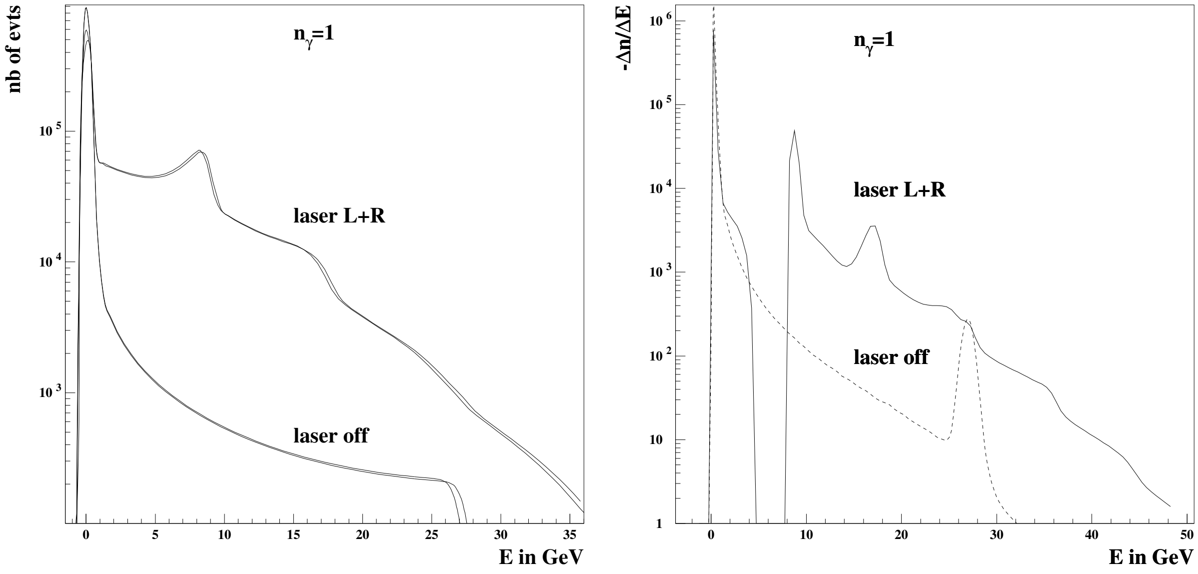

Figure 5: Left: Simulated spectrum as seen with the LPOL in the few photon mode and with high statistics. Clearly seen are Compton-edges due to one, two and three photons observed in the detector, and the brems-edge from the background. Right: Differentiated spectrum, as could be used to determine the position of the one, two, three photon peaks and the brems-background edge. The different peaks are clearly visible, and allow a calibration of the energy scale to better than 1%.

3.2 The Fabry-Perot Cavity

The basic setup of a Fabry-Perot cavity consists – in our case – of two spherical mirrors set opposite each other. Each mirror is made of a silica substrate with a thin dielectric coating on the inner spherical surface (see A.3 for details). For comparison is it useful to define the power inside the cavity as the power which a CW laser would need to obtain the same Compton scattering rate as the beam inside the cavity. Assuming a transverse Gaussian mode of the laser this power P_{in} inside the cavity is given by:

$$P_{in} = P_0 \times G \ , \ G = \frac{T}{(1-R)^2} \times \frac{1}{1 + \frac{4R}{(1-R)^2} \sin^2 \frac{2\pi\nu L}{c}}$$

where G is the cavity gain, T and R are the transitivity and the reflectivity of the coating respectively, and L is the cavity length. R and T are related by

$$R + T + D + A = 1$$

where A and D are the absorption and diffusion coefficients of the coating. The maximum gain is given by: $G_{MAX} = T/(1-R)^2$ for a laser frequency $\nu = \nu_0 \equiv n \times c/2L$ and the free spectral range (distance between two resonance peaks) is $c/2L$ (which is $\approx$ 75MHz for a 2 m long cavity).

In figure 6 (right) the calculated gain of the cavity used in the CEBAF polarimeter is shown. On the resonance it reaches a gain of a few times 10^3 for $R = 0.99988$ and $T = 0.00012$ for infrared light with $\lambda = 1064$ nm. At CEBAF gains of larger than 7000 have been achieved, very close to the expected theoretical performance.

Using a low power laser of $P_0 \approx 1$ W, very high levels of power around $P_{in} \approx 10$ kW can be reached inside the cavity. With such a system the required power to obtain a high enough photon flux to operate the system in the few photon mode can be reached.

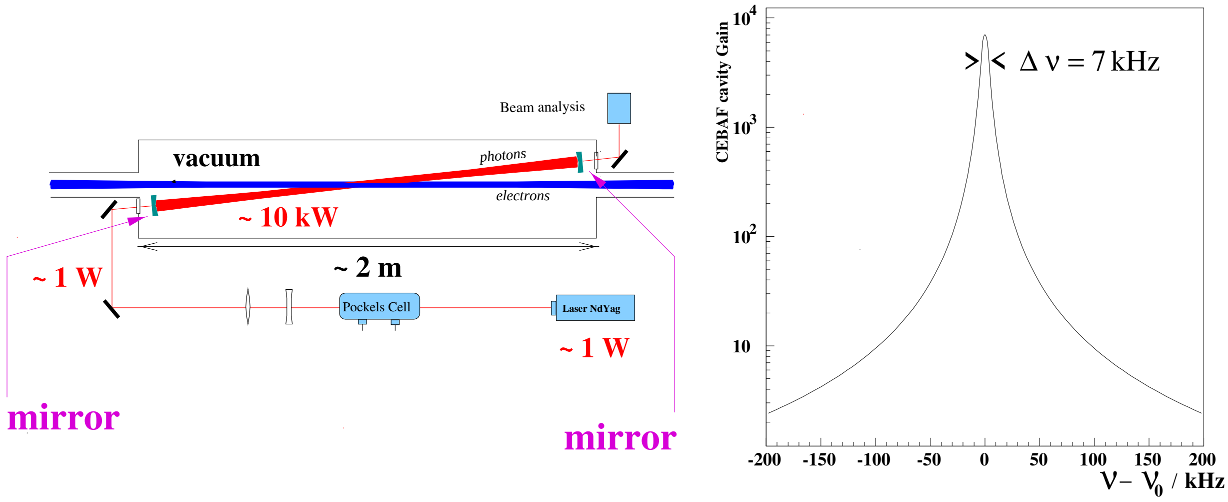

Figure 6: Left: Simplified scheme of a Fabry-Perot cavity and laser system located around the electron beam. The power indicated in the cavity is the equivalent power a CW laser must deliver to obtain the same Compton scattering rate. The power values give the order of magnitude of the laser power inside the laser, outside the laser and inside the cavity. Right: Gain of the cavity used at the CEBAF accelerator to measure the electron beam polarization (see text).

3.2.1 Choice of the Laser

The choice of the laser frequency is governed by a number of different criteria. The wavelength determines directly the distance between the background and the signal (Compton edge). A larger wavelength, corresponding to a lower photon energy, results in a smaller separation between signal and background. On the other hand, due to the increasing Compton-cross section at smaller energies, the number of backscattered photons at constant laser power and constant lepton beam current increases. In figure 3 the spectra for a green laser operating at 532 nm and for an infrared laser operating at 1064 nm are shown. Both effects are clearly visible.

Equally important is the influence of the laser wavelength on the required precision of the cavity. This will be explored in detail in section 3.2.2 and 3.2.3. However as a general statement a longer wavelength sets less stringent requirements on the mechanical tolerances of the cavity than a shorter wavelength.

The expected performance of the polarimeter has been studied for both green and infrared lasers. The study was done using a beam polarization of 50%, and assuming lasers with the same beam power. The ratio of the polarization precision for green over infrared laser is shown in figure 7. From the figure it is clear that the infrared laser performs better than the green laser in all instances. Coupled with the less stringent mechanical requirements for a cavity operated in the infrared, we propose to use an infrared laser operating at 1064 nm for the LPOL.

Such lasers are commercially available from the Lightwave company. The chosen model is a tunable infrared laser, where the laser frequency can be changed by 30 GHz (30 MHz) through a coarse (fine) adjustment mechanism. Such a laser has been successfully employed in the CEBAF setup.

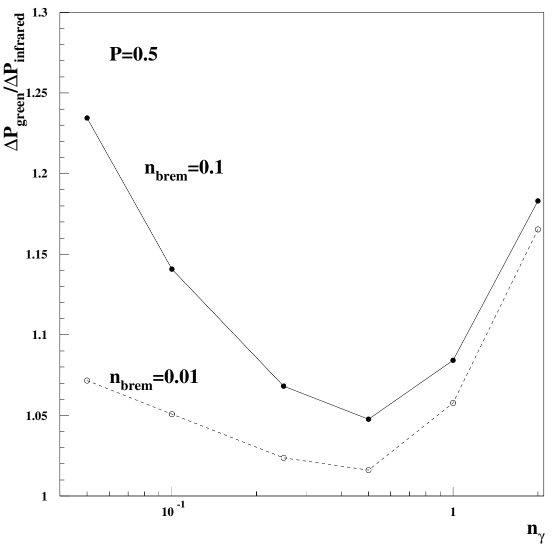

Figure 7: Ratio of polarization precision for green and infrared lasers for 10% and 1% background, as a function of the probability to get a backscattered photon from one bunch.

3.2.2 Choice of the cavity geometry

The exact layout of the cavity is determined by the total distance between the two mirrors, by the curvature of the mirrors, and by the crossing angle between the laser and the lepton beam. The conceptual design of the cavity is a close copy of the one installed at CEBAF.

The laser - lepton beam luminosity can be written as

$$\mathcal{L}_{e,\gamma} \approx \frac{1}{\sqrt{2\pi}} \frac{1+\cos\alpha}{\sin\alpha} \frac{I_e}{ec} \frac{P_{in}\lambda}{hc} \frac{1}{\sqrt{\sigma_{e,x}^2+\sigma_\gamma^2}} , \tag{4}$$

where $\lambda =$ is the laser wavelength, P_{in} is the power inside the cavity, $\sigma_{e,x} = 0.94mm$ is the largest electron r.m.s. beam width in the section where we could locate the cavity [10], $\sigma_\gamma = w_0/2$ is the laser width ($\sigma_\gamma^2 = L\lambda/(2\pi)$ for a confocal cavity see section A.2), I_e is the electron beam current, α is the $e-\gamma$ crossing angle: $\alpha = 2d + \Phi/L$, L is the cavity length, d is the distance between the electron beam axis and the edge of the mirror (see also fig. 18) and Φ is the mirror diameter. The minimum value for d is 2 cm (beam pipe radius in y) plus 2.5 cm for mechanical purposes. We take $d = 4.5$ cm. The mirror diameter is 2.5 cm.

The luminosity is directly related to the number of backscattered photons through the formula:

$$n_\gamma/bunch/mA = \frac{\mathcal{L}_{e,\gamma}}{I_E}\sigma_c[barn] \times 96 \cdot 10^{-9} \tag{5}$$

where σ_c is the total Compton cross-section above the energy threshold $E_\gamma > 2$ GeV, $\sigma_c =$ 0.37 nb for infrared light.

Parameters to optimize the luminosity are the length of the cavity and the mirror curvature. In the following we assume that the cavity is a con-focal cavity ($L = R_c$).

In Figure 8 the effects on the number of backscattered photons are shown when the length is varied. The grey hatched area corresponds to the targeted photon rate of 1 to 2 photons per interaction for an electron current of 40 mA.

From the plots it can be seen that a 2 m long cavity intersecting the lepton beam at 3.3 degrees (58 mrad) will deliver the needed luminosity. Such a cavity represents a modest extrapolation from the CEBAF cavity, which is only 1 m long.

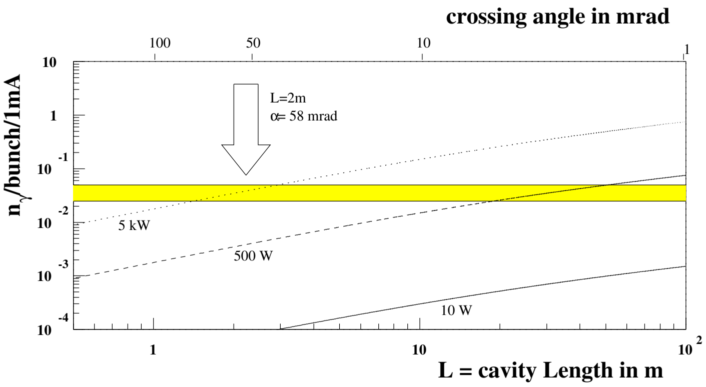

Figure 8: Event rate per bunch normalised to a total electron current of 1 mA as function of the cavity length (bottom scale) and the crossing angle (top scale). For the plot it is assumed that the separation between the beam axis and the mirror center is kept constant at 5.75 cm.

3.2.3 Mechanical Design of the Cavity

A layout of the preliminary design of the cavity is presented in figure 9. Two spherical mirrors are supported by a big and solid support tube at a distance of 2m in such a way that a laser beam captured between the mirrors crosses the electron beam at an angle of 3.3 degrees. The beam from an external laser is coupled into the system through a quartz window, and a beam is extracted from the cavity through a second quartz window at the opposite end of the system. The vessel is under vacuum and kept at the same pressure as the beampipe. Presumably special pumping needs to be foreseen to maintain the vacuum inside the vessel.

One of the main considerations when designing the cavity is that wake fields from the passing electron beam should not disturb the cavity operation, and that the cavity should not interfere with the electron beam. The mutual interference is minimized by the introduction of a 15 mm diameter tube, which is used to suppress the propagation into the cavity of high frequency modes from the passing beam. Preliminary calculations indicate that this tube should extend ±80 cm from either side of the hole in the beam pipe. By making the hole for the laser beam in the beam pipe as small as possible the power loss through electromagnetic heating is also reduced to an almost negligible level (18 W during injection, less than 0.1 W during normal beam operation [11]).

It is foreseen that the existing copper beampipe is replaced by a few meters of stainless steel beampipe, to which the cavity elements are added. The special cavity beampipe is then connected to the normal HERA ring through a system of standard vacuum bellows, to suppress the transmission of acoustical vibrations from the ring into the cavity system.

To minimize the temperature variations during operation the whole setup should be installed inside an enclosure which has some level of temperature stabilization. Since for safety reasons the laser anyway needs to be installed in a closed box, this does not introduce any additional complications.

A possible place for the installation of such a cavity exists downstream of the current polarimeter, between the quadrupoles 61QL16 and 67QL17 (about 62 m from the HERMES interaction point). There approximately 4 m of straight section exist, equipped only with the standard getter pumps. Installation of the cavity at this location would interfere minimally with the HERA machine, would allow the continuing operation of the existing LPOL, and makes the use of the existing photon detector for both the old and the new LPOL possible.

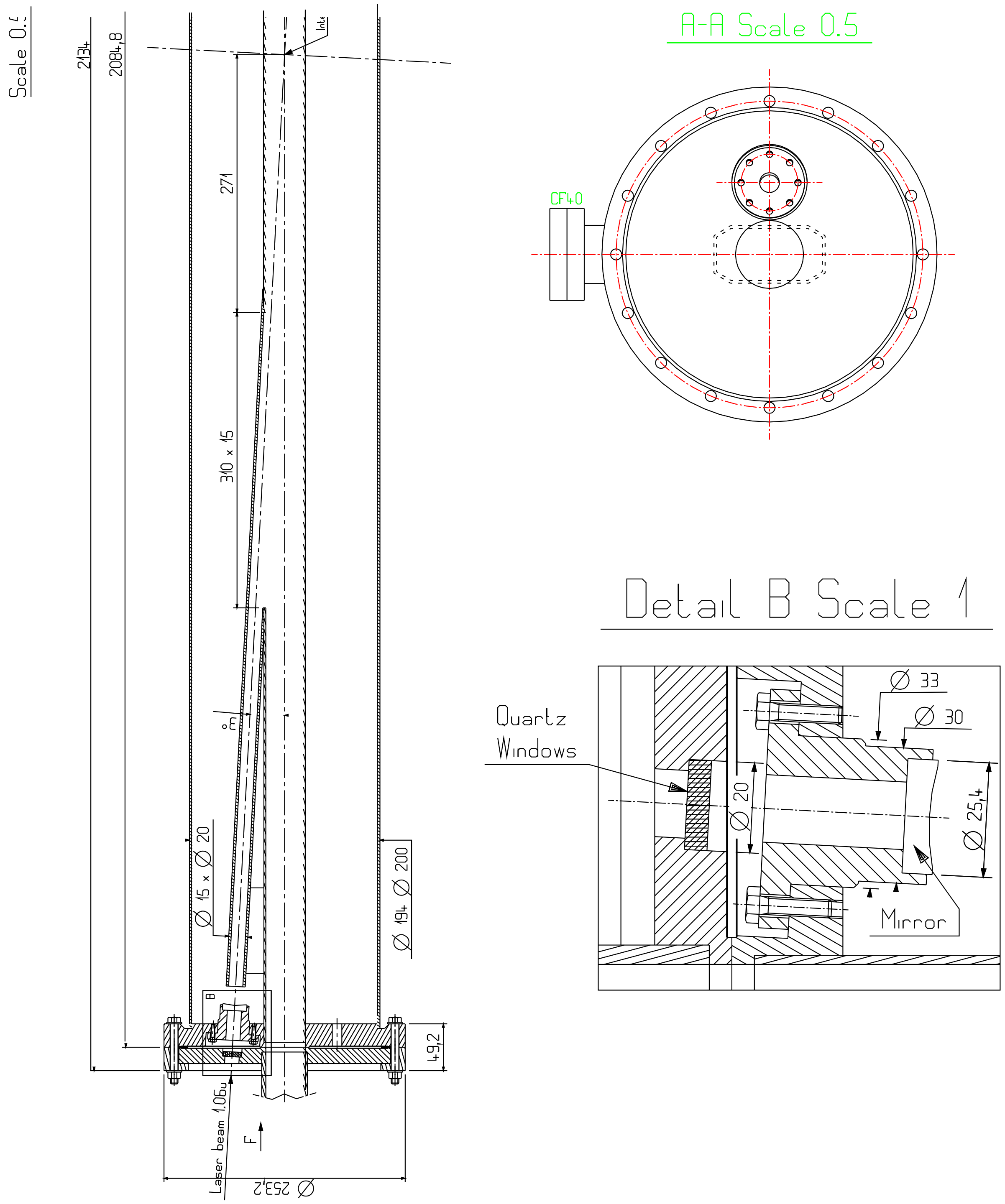

Figure 9: Preliminary layout of the HERA cavity. Only one half of the cavity is shown.

3.2.4 Mechanical Details for a Monolithic Cavity

Detailed studies have been made to understand the level of mechanical precision needed to successfully operate the Fabry-Perot cavity. Three main aspects need to be considered:

- the optical elements of the cavity need to be properly aligned and kept in alignment to ensure that the resonance condition is maintained;
- the laser beam has to be coupled into the cavity with sufficient precision, so that resonance occurs;
- the cavity itself has to be aligned with respect to the HERA beam in such a way that the photon beam and the lepton beam intersect.

The cavity might be influenced through thermal effects which change the length of the cavity, vibrations which might change the length and result in tilts of the mirrors, and possible fabrication imperfections, resulting in wrong alignment between optical components.

Any misalignment may result in total loss of the resonance condition, or at least reduce the power in the cavity. Studies (see appendix A.4 for details) have shown that if the tilt of the mirrors relative to the perfect optical axis is kept below some mrad, and if the optical axes of both mirrors are aligned to better than around 0.5 mm, a beam can be maintained in the cavity without significant losses.

The large power of the laser beam inside the cavity might heat the mirrors, distort them, and thus change the cavity properties. Calculations have shown that such effects are expected to be rather small, and should at most result in a power loss in the cavity of less than 2%.

To maintain the cavity in resonance even for perfectly aligned mirrors, the distance between the two mirrors expressed as the number of the wavelengths of the laser beam needs to be tightly constrained. This condition can be much relaxed if a frequency tunable laser is used, as proposed. Based on the adjustment range of the chosen laser a length variation of around 70μm can be absorbed without problems. If larger length variations are encountered, the cavity might start to oscillate in a different mode, which will complicate the situation significantly.

The main effect which might change the length of the cavity is an expansion or contraction of the cavity due to temperature variations. A $70 \mu m$ variation in the length corresponds to a temperature change of about 2.0K, if the cavity is constructed from stainless steel, or approximately a factor 10 more, if a special material with a low expansion coefficient is used. With the above mentioned temeperature stabilized enclosure this should not present any problems.

From these studies it is concluded that it should be possible to construct and operate a Fabry-Perot cavity in the HERA environment without major problems.

3.3 Data Acquisition System

The significantly higher rates with which data are taken with the new LPOL make an addition to the existing data acquisition system necessary. We propose to continue to use the existing slow controls and monitoring system, and to only add a fast DAQ system to record and analyze the data from the few photon operation of the LPOL. This option can be most easily implemented since it can profit heavily from the existing infrastructure and from the new data acquisition system for the TPOL which is currently under development. The only difference to the TPOL system is that the new LPOL system needs to be optimized for larger speed with a smaller number of channels.

In this basic option the new LPOL DAQ consists of two almost independent subsystems:

- a laser and cavity control system and its auxiliary electronics for laser alignment, feedback control, switching and monitoring of the cavity power and polarization. This system is a close copy of the system developed for the CEBAF polarimeter;

- a VME based fast DAQ system for the few photon mode LPOL, which is a close copy of the TPOL fast DAQ.

The control of the photon detector will be done through the existing DAQ for the multi photon LPOL.

3.3.1 Fast LPOL DAQ

The fast part of the DAQ for the new LPOL is a close copy of the system which is currently being built for the TPOL. In essence it consists of custom-made fast ADC's and TDC's, which are read out by a dedicated Power-PC based controller (MFCC), while a second Power-PC takes care of the analysis and control of the data. The ADC planned for the TPOL is fast enough to handle the amount of data from the new LPOL. A slightly more sophisticated pipelining scheme will have to be employed to handle the larger total data rate in the readout.

3.3.2 Laser and Cavity Control

The more challenging part of the proposal is the system needed to operate and monitor the cavity. We propose to use an exact copy of the system developed for the CEBAF polarimeter.

The laser control system has two operation modes: manual and automatic. Under manual control the operator has direct control of the moving parts with corresponding data displays. Under automatic mode the following procedures are implemented:

- Laser Feed Back Startup: The feedback electronics is started and the finding of the resonance is monitored.
- Laser Beam Alignment: 4 mirror motors, 8 monitoring diodes from 2 four cell quadrants, and beam transmission monitors are used to control the laser beam. A CCD camera permits a visual control of the resonant modes present in the cavity.
- Run Control: Based on instructions received from the main run control, parameters like the light polarization, the power etc are varied and monitored.

All components in the system are commercial components, except for the laser feedback electronics.

3.3.3 Laser Feedback Electronics

The laser feedback electronics consists of three modules and a cavity monitoring diode and its preamplifier, located in the HERA tunnel close to the cavity.

The whole system is shown in figure 10. The role of the electronics is to control the frequency of the laser by adjusting the length of the laser rod. Two different means of adjusting the frequency exist, a coarse one and a fine one. The length of the laser rod is primarily controlled through its temperature. A Peltier element is used to change the temeperature of the laser rod. The voltage applid to the Peltier element is fixed through a "slow feedback" signal provided at a level of a few Hz. Fast, small variations in the frequency are obtained by applying a mechanical pressure to the laser rod through a piezo-electric element.

This system can operate in two modes:

- "open loop" mode: If no resonance is detected a ramp signal is applied to the crystal. If a crossing of the resonance frequency is detected, the sequencer card switches the system to the "closed loop" mode;

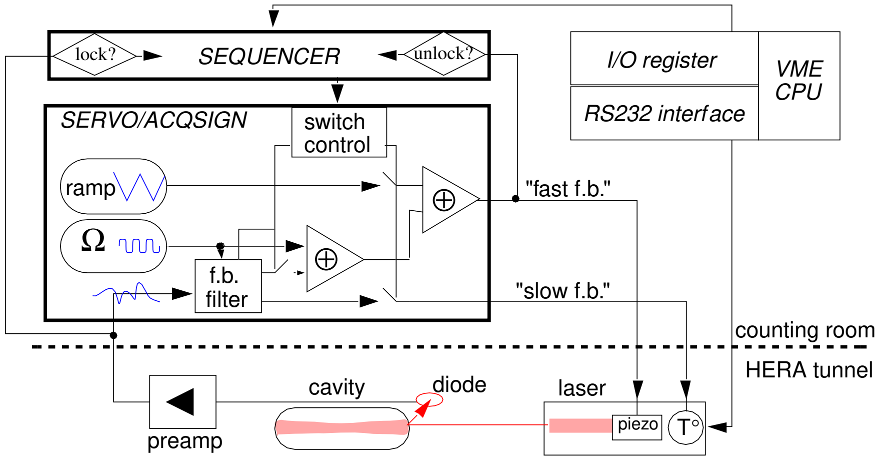

Figure 10:

- "closed loop" mode: The crystal is vibrating continuously at $\Omega = 1$ MHz with a very small amplitude. The phase shift excursion during one period of $1\mu s$ is small compared to $\pm\pi/2$, and the resulting power loss in the cavity is negligible for normal operation conditions. However the power loss can be detected in the beam behind the cavity, and used to calculate an error signal which indicates how far the system is away from an ideal resonance condition. A correction signal is the fed back to the piezo-electric crystal ("Pound-Drever" method). If a perturbation is encountered to break the closed loop, the sequencer raises an "unlock" status, and the open loop scan is restarted automatically.

As all modules necessary for the operation of the cavity have already been developed and are used in the CEBAF polarimeter, the system can be assembled in close collaboration with Saclay's CEBAF team.

3.4 System Layout

The overall layout of the system is presented in figure 11. This is essentially a copy of the CEBAF system. Further modifications to fit the system into the HERA tunnel can and will be made and should not present any basic problems. The laser beam is produced in the low power IR laser from the Lightwave company. The laser is optically isolated from the rest of the system through a Faraday insulator. The laser light is circularly polarized in a Pockel-cell. The laser beam is brought into the cavity by 2 motorized mirrors (M1 and M2) and three fixed mirrors (Mr1, Mr2, Me). The cavity is formed by the mirrors Mce and Mco, which are also fixed. The Plates L1, L2 and L3 are used to adjust the beam properties and the waist in the interaction point. Up to Mr2 the laser beam is kept in a plane below the beam pipe. It is then reflected upwards by the mirrors Mr2 and M2 above the beamline. Me and Mce are located above the beam line, Mco and Mo below the beamline.

Behind the cavity a number of optical elements are located to monitor the beam quality, measure the intensity and the polarization in the cavity.

The elements SC, S3 and the fast photo-diode PDR are used in the feedback mechanism described earlier.

The whole system can be installed on an optical table of approximately 40 x 200 cm. This table has to be installed below the current HERA beam pipe.

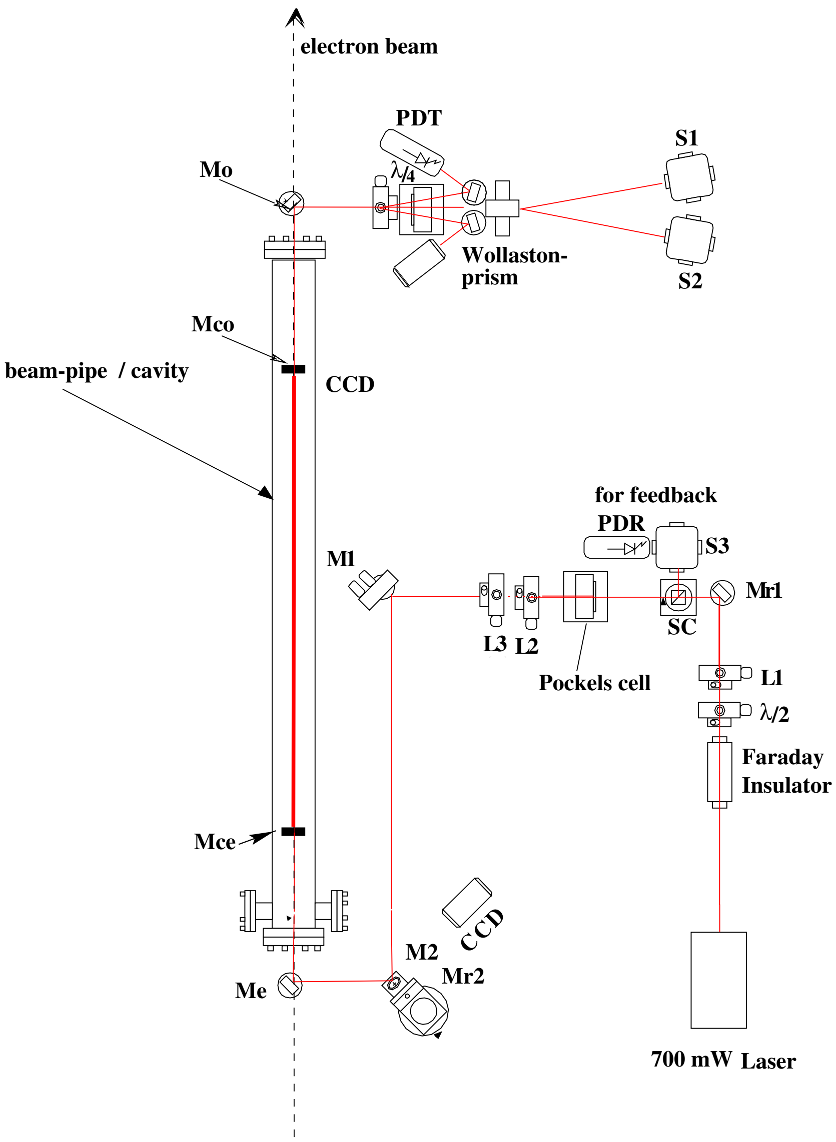

Figure 11: Conceptual layout of the cavity and laser system as proposed for the HERA tunnel

3.4.1 Cost, manpower and schedule

In Table 2 a breakdown of the cost for this project is given. The costs are to be considered preliminary, and more research is needed to find the optimum and most cost effective solution. The table does not include contingency nor manpower costs provided by the institutes.

To install the cavity in the HERA tunnel a number of additional components are necessary. The old beam pipe needs to be replaced by a new stainless steel one over a distance of approximately three meters. The connection between the existing HERA beampipe and the cavity beampipe has to be made through a pair of bellows. Some civil engineering will be needed to prepare the installation of the optical table under the electron beam pipe. Services like cooling, electricity etc will have to be provided.

The LAL is ready to consider the design and construction of the cavity and its associated equipment. It is expected that DESY and other members of the POL2000 group can contribute to the installation and the preparation of the infrastructure needed for the cavity. In addition significant funds are available through a DFG project in collaboration with Russian groups involved in the H1 experiment. Their expertise, in particular in optics and in data

item		quantity	price (in kEuro)
laser (0.7W tunable)		1	40
optical table	main table	1	5
	legs	4	4
	subtables	3	4
optical components	lenses	5	2
	$\lambda/2$ plate	1	0.5
	Pockels-cell	1	2
	motorised mirrors	3	24
	photo meter	2	8
	intensity meter	2	7
	Faraday insulator	1	3
	holographic beam sampling	1	2
	Wollaston prism	1	1
Cavity	mirrors	2	25
	entry/exit windows	2	10
	mechanics	-	50
Electronics	cavity feedback	1	12
	DAQ	1	20
	Sum total		≈ 220

Table 2: Breakdown of the costs for the cavity project. Not included are contingency and manpower costs. Prices are in 1000-Euro.

analysis, will be relied on heavily. Work related to the data acquisition, analysis etc will, to a large extend, profit from work already under way for the upgrade of the TPOL.

Given the resources available for polarization, the dense schedule of the HERA upgrade and other considerations we propose to aim for an installation of the cavity in the first longer shutdown after the luminosity upgrade, probably at the end of 2001. It is unlikely that both high luminosity and high polarization will be achieved in the first months after the luminosity upgrade.

Construction of the cavity could start in principle in the second half of this year, which would leave approximately one year to build and commission the cavity as a table top experiment. Installation in HERA should not present insurmountable problems, if proper preparation for the necessary civil engineering can be done in advance.

3.5 Conclusion

We have presented the outline of a project to install a Fabry-Perot cavity at the LPOL so as to significantly increase the power of the HERA polarimeter system. The main advantages of the proposed new system are a much larger statistical precision, and the capability to have a self-calibrating device.

We propose to install a system which is very closely modeled on an existing system at CEBAF. This essentially eliminates the need for special R&D and minimizes the risk connected to any new installation in the ring. We propose to install the system next to the existing LPOL system, so that both can be operated in parallel.

We are convinced that a high precision measurement of the polarization with related excellent control of the systematic errors of the polarization will become an increasingly important part of the HERA physics program. We think that the proposed addition to the existing polarization program offers a safe and adequate route to achieve this goal.

A Appendices

In the following appendices detailed investigations into the properties of the Fabry-Perot cavity are presented. The conclusions from these studies were already presented in the main body of this note.

A.1 Physics of the Fabry-Perot Cavity

Inside an isotope homogeneous medium the Maxwell equations read as:

$$\nabla \times \mathbf{E} = -\frac{\partial \mathbf{B}}{\partial t} \; ; \; \nabla \times \mathbf{H} = \frac{\partial \mathbf{D}}{\partial t}$$

with $\mathbf{B} = \mu\mathbf{H}$ and $\mathbf{D} = \epsilon\mathbf{E}$. This leads to the electric field propagation equation:

$$\Delta \mathbf{E} = \epsilon\mu \frac{\partial^2 \mathbf{E}}{\partial t^2} \,. \tag{6}$$

Well known solutions to this equation are the plane waves or the spherical waves. However, a laser beam, being produced inside a cavity, cannot be easily described in the plane waves or spherical waves basis: high quality laser beams have a Gaussian transverse profile. There is therefore a revolution symmetry around the wave propagation axis z and it is useful to express the solution of eq. (6) in term of the Hermite or Laguerre polynomials. A perfect Gaussian transverse beam is described by the first order Hermite or Laguerre polynomials (= fundamental mode) which are equivalent but, when some defects appear (= when the axial symmetry is broken), higher order polynomials contribute to the expression of the transverse electric field (= higher modes are excited). If the symmetries with respect to the $x = 0$ and $y = 0$ planes are not broken the Hermite polynomials are used. If the system presents a first order rotation symmetry, then the Laguerre polynomials are used.

The calculations can be found in [12] (a summary can be found in [13, 14]). The main perturbations described in this proposal generate the modes shown in fig. 12.

When a higher mode is coupled into a Fabry-Perot cavity through a laser beam, the resonance frequency is changed. Therefore, if the resonance frequency is adjusted to that of the fundamental mode, the exited modes will not penetrate inside the cavity and will only induce a power loss.

A.2 Laser intensity and various definitions

For a Gaussian transverse mode, the electric field reads:

$$\mathbf{E} = \mathbf{E}_0 \frac{w_0}{w(z)} e^{i\eta(z)} e^{ik\rho^2/2R(z)} e^{-\rho^2/w^2(z)} e^{i(\omega t - kz)}$$

and the corresponding laser intensity inside the cavity is given by:

$$I(\rho, z) = \frac{2P_{in}}{\pi w^2(z)} \exp\left[-\frac{2\rho^2}{w^2(z)}\right]$$

where

- P_{in} is the power inside the cavity;
- z is the cavity optic axis, $z = 0$ at the center of the cavity;
- $\rho^2 = x^2 + y^2$;

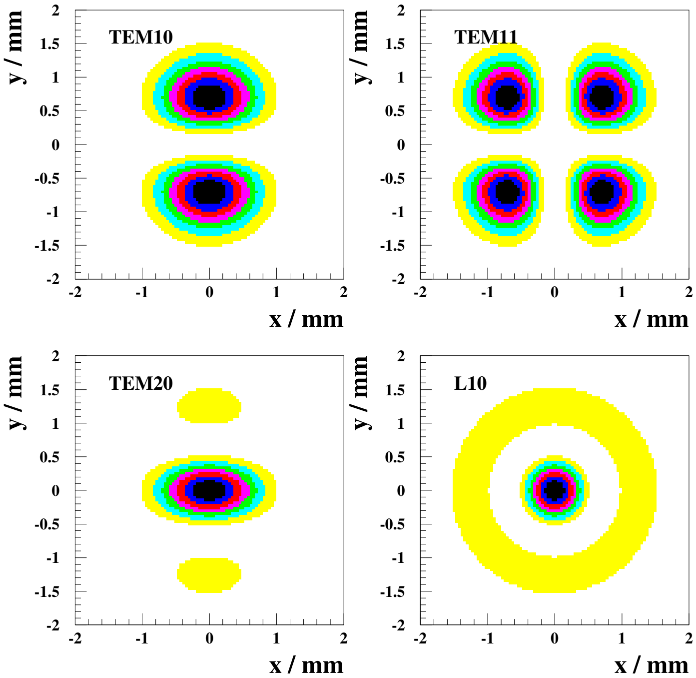

Figure 12: Excited transverse mode appearing when the axial symmetry is broken. TEM10, TEM11 and TEM20 refer to the Hermitte polynomials and L10 refers to the Laguerre first order polynomial.

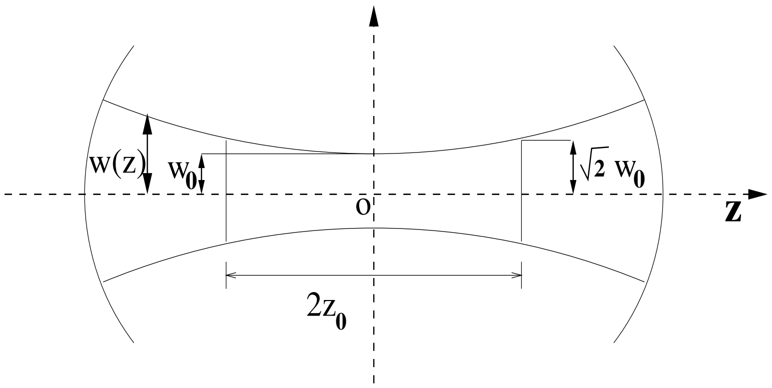

Figure 13: Beam radius $w(z)$ and its minimum (waist) w_0 inside a Fabry-Perot cavity.

- $w(z)$ describes the transverse size of the laser beam (see fig. 13), as a function of z (the one standard deviation of the laser beam intensity distribution is given by $\sigma_\gamma(z) = w(z)/2$):

$$w(z) = w_0\left[1+\frac{z^2}{z_0^2}\right]^{1/2}; \;\; z_0 = \frac{\pi w_0^2}{\lambda}$$

  For $z = 0$ one has $w(0) \equiv w_0$ (w_0 is the laser beam waist); z_0 is the Rayleigh range.

- $\eta = \tan^{-1}(z/z_0)$ is a phase factor.

- $R(z) = z + z_0^2/z$ is the real part of the wave radius of curvature.

In a cavity where the two mirrors are similar the waist is minimum at the center of the cavity.

The resonance occurs when the laser beam waist is adjusted to the cavity waist. The adjustment is obtained by using motorized mirrors at the entrance of the cavity. For two identical spherical mirrors, the cavity waist is given by:

$$w_0 = \sqrt{\frac{\lambda}{2\pi}(L(2R_c - L))^{1/4}}$$

It depends on:

- λ= laser wavelength
- L= cavity length
- R_c= radius of curvature of the mirrors (see section A.3). Here the two mirrors are assumed to be similar.

An important quantity is the finesse

$$F = \frac{\pi\sqrt{R}}{1-R}$$

which is roughly the number of plane wave reflections inside the cavity

A.3 The mirrors

A scetch of the mirrors is given in fig. 14.

The two identical spherical mirrors of the cavity are characterized by the following quantities:

- The coating, made of dielectrics layers SiO_2 ($n = 1.47$) / Ta_2O_5 ($n = 2.1$).
- The substrate made of silica SiO_2.
- R_c = radius of curvature ≈ 2 m [15].
- Φ = diameter ≥ 2.5 cm[15].
- R_u the useful radius (size of the coating in the substrate) ≈ 10 mm.
- Absorption coefficient of the coating,
  $A \approx 5ppm$ for green light and $A \approx 1$ ppm for infrared light.
- Diffusion coefficient $D \approx 2$ ppm of the coating (it depends on the surface defects of the coating).

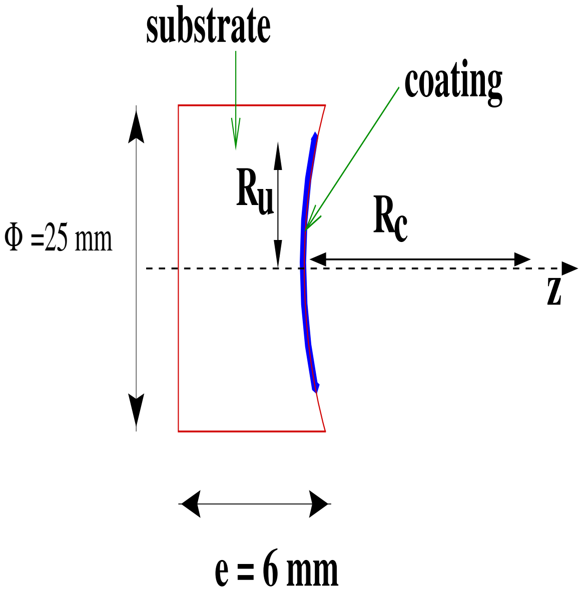

Figure 14: Simplified scheme of the mirror (see text).

- Thickness of the substrate $e = 6$ mm (the thickness of the coating is negligible with respect to the substrate thickness).
- Absorption coefficient of the substrate $A_s \approx 1$ ppm/cm for high quality silica (as used by VIRGO).

Because of the nonvanishing absorption of the coating, there is a maximum laser intensity that the mirrors can tolerate. For a Gaussian laser beam, the maximum intensity on the mirrors is localized at $\rho = 0$:

$$I_{max} = \frac{2P_{in}}{\pi w^2(z = L/2)}$$

and it amounts to [15]:

$$I_{max} \quad = 40kW/cm^2 \times 200 \times \tfrac{1}{2} \equiv 4MW/cm^2 \text{ for red light}$$

- The 40kW comes from a study made with a pulsed laser of 600 nm;
- the factor 200 is to go from pulsed to continuous laser mode.
- the factor 1/2 is for security

This number is used in section 3.2.2 where the luminosity is optimized.

A.3.1 Mirror heating

A high intensity laser beam beam inside the cavity induces temperature variations inside the mirror substrate. Various effects – due to a temperature gradient inside the substrate – must be considered [16]: the surface of the substrate is modified (thermoelastic effect) inducing a modification of coating as well; the substrate optical indices is modified inducing an optical path distortion.

The heat propagation equation is difficult to solve. We have used the analytical solutions obtained in ref. [17, 18] where the following boundary conditions are applied: radiative loss on all the mirror surfaces and a Gaussian transverse intensity in the coating. As shown in section 3.2.3, the mirrors are in contact with a heat conducting support so that at the boundary the solution is dominated by the heat conduction and not by radiative dissipation. Nevertheless, since the silica is a weak conductor, the temperature gradient obtained with the real boundary conditions is very close to the one obtain using the analytical solution. This point was tested numerically [19] for the steady solution: we found that if the substrate is surrounded by a conductor in perfect connection with the silica, the temperature inside the silica is approximately reduced by 1 K only.

The characteristic time of thermal effects is given by [16] $t_c = \rho_s C \Phi^2/4K$ where ρ_s is the silica density (2202 kg m^{-3}), C is the specific heat (745 J kg^{-1}), K is the thermal conductivity (1.38 W m^{-1}K^{-1}) and Φ is the substrate diameter. Taking $\Phi = 2.5$ cm one gets $t_c \approx 3$ min. Since this time is of the order of a minute, not only the steady solution of the heat propagation equation but also the transient solution must be studied.

Concerning the medium, the two crucial parameters are the dielectric absorption coefficient A and the silica absorption coefficient A_s. We take $A = 1$ ppm for infrared light (note that $A = 5$ ppm for green light) and $A_s = 1$ ppm/cm. The notations are defined in fig. 15.

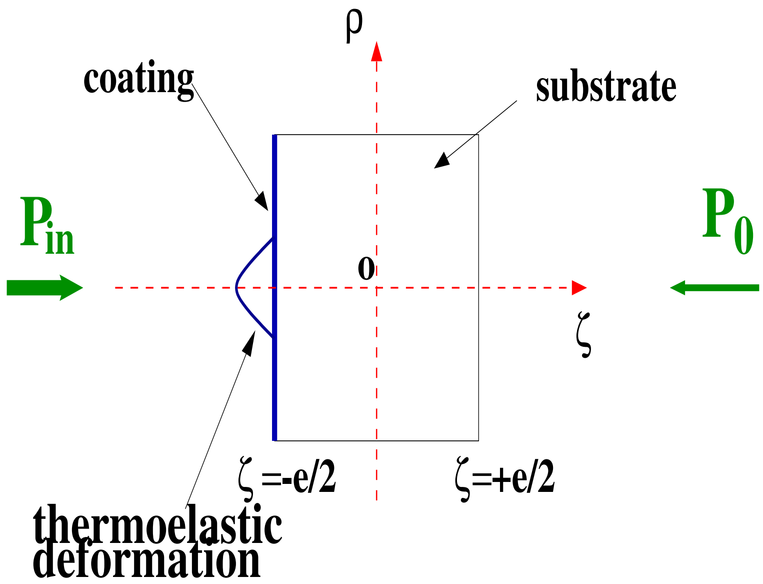

Figure 15: Definition of the notation used to compute the heat propagation in the mirrors.

To estimate the temperature effects we have considered a con-focal monolithic cavity of 2 m length ($R = L = 2$ m), the wavelength $\lambda = 1064$ nm, an ambient temperature $T_0 = 300$ K. In order to get a conservative estimate we have set the power inside the cavity to $P_{in} = 10$ kW. The mirror diameter is fixed to $\Phi = 2.5$ cm and the substrate thickness to e = 6 mm (the coating thickness is neglected).

It is to be mentioned that heat is produced both by the power inside the cavity and by the incoming power. In the former case, the 'transmitted' power is given by $P_{in} \times A$ and in the latter case by $2 \times P_0 \times A_s \times e$. Using the numbers given above one can safely neglect this latter case.

Due to radiative thermalisation, the mirror is at ambient temperature when no beam is circulating inside the cavity. The results of our calculation are presented in figure 16. We first show the temperature increase when the stationary state is reached. In the two following figures we give the results of the temperature increase as a function of $\rho = \sqrt{x^2 + y^2}$ ($\rho = 0$ at the center of the mirror) and ζ, the position on the z axis inside the substrate ($\zeta = 0$ at the center of the substrate). The largest temperature increase is located essentially in the center of the mirror close to the coating and reaches T_0+4.5 K at the hottest point. The steady state is reached after 10s, so that already after a very short time the system is operated in a stable state.

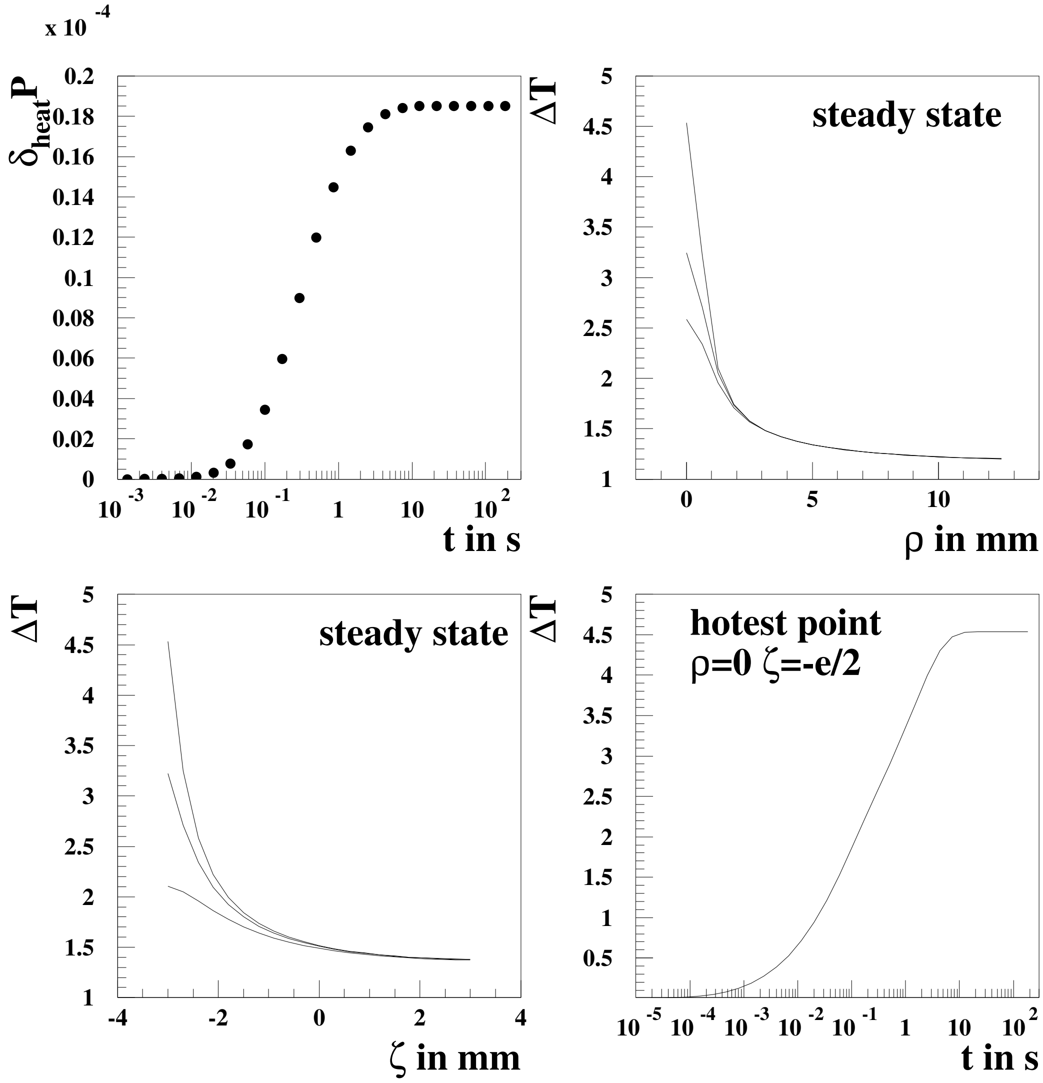

Figure 16: Upper left: power lost due to variations of the index of refraction induced by the temperature gradient inside the substrate as a function of time. Upper right: temperature variation in steady state as a function of ρ for $\zeta = -e/2 = -3$ mm (upper curve), $\zeta = -2.7$ mm and $\rho = -2.4$ mm (lower curve). Lower left: temperature variation in steady state as a function of ζ for $\rho = 0$ (upper curve), $\rho = 0.625$ mm and $\rho = 1.25$ mm (lower curve). Lower right: temperature variation as function of time at the hottest point $\zeta = -e/2$ and $\rho = 0$.

A.3.2 Thermoelastic effect due to absorption in the coating

Results for the thermoelastic deformation are shown in fig 17. The time scale of this effect is about 10 s and it induces a sagitta of about 2 nm at the hottest point ($\zeta = 0$ and $z = -e/2$).

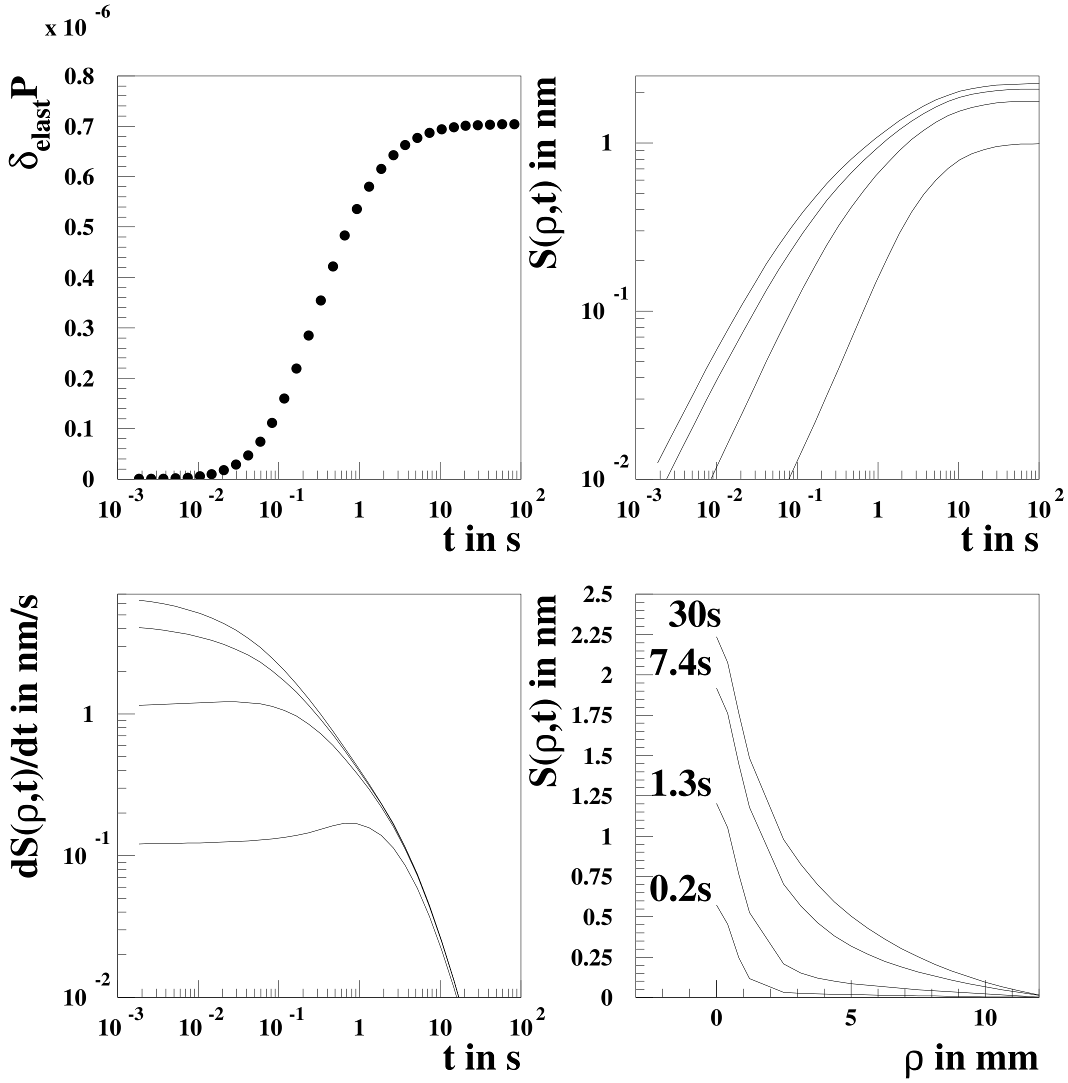

Figure 17: Up-right: power lost after one reflection on the coating as function of time. Up-right: thermoelastic deformation of the coating $S(\rho, t)$ as function of time for $\rho = 0$ (upper curve), $\rho = 0.4$ mm, $\rho = 0.8$ mm and $\rho = 2.5$ mm (lower curve). Down-left: time derivative of the thermoelastic deformation $dS(\rho, t)/dt$ as function of time for $\rho = 0$ (upper curve), $\rho = 0.4$ mm, $\rho = 0.8$ mm and $\rho = 2.5$ mm (lower curve). Down-right: thermoelastic deformation of the coating $S(\rho, t)$ as function of ρ for different values of t.

If the thermoelastic deformation of the coating is not a quadratic form in ρ, power is lost at each reflection of the light inside the cavity. An estimation of this loss as function of time is given by the projection of the modified transverse field onto the fundamental TEM00 mode [16, 18]:

$$\delta P_{\text{elast}}(t) = 1 - \left| 2\pi \int_0^{\Phi/2} \exp\left(-2i\pi S(\rho, t)/\lambda\right) |\psi_{00}(\rho)|^2 \rho d\rho \right|^2$$

where $\psi_{00}(\rho) \propto \exp\left(-2\rho^2/w^2(z)\right)$ (see section A.2). The result of this estimation is shown in fig. 17. Multiplying $\delta P_{\mathrm{elast}}(t)$ by the number of wave plane reflections (= the cavity finesse $F \approx 26000$) one finds a total power loss of $\approx 1.8\%$.

A.3.3 Modification of the substrate indices

A high temperature inside the substrate modifies the optical index of the substrate. If this modification is not a quadratic form in ρ, power is lost when the incoming laser beam enters the cavity. An estimation of this loss as function of time is given by [16, 17]

$$\delta P_{heat}(t) = 1 - \left| 2\pi \int_0^{\Phi/2} \exp\left(-2i\pi\Psi(\rho,t)/\lambda\right) |\psi_{00}(\rho)|^2 \rho d\rho \right|^2$$

where $\psi_{00}(\rho)$ is given in section A.2 and where the optical path distortion is given by:

$$\Psi(\rho,t) = \frac{dn}{dT}\int_{-e/2}^{e/2} T(\rho,\zeta,t)d\zeta$$

($dn/dT = 8.710^{-5}$ K^{-1} is the silica thermal coefficient of the index). The result of this estimation is presented in fig. 16. It is a negligible effect.

A.3.4 Birefringency induced by heat is the substrate

Heat inside the substrate induces a birefringency of the substrate. This effect has been estimated and studied (see [16] and ref. therein). It affects only the incoming light and it was found to be negligible at around 0.01%.

A.4 Mechanical tolerances for a monolithic cavity

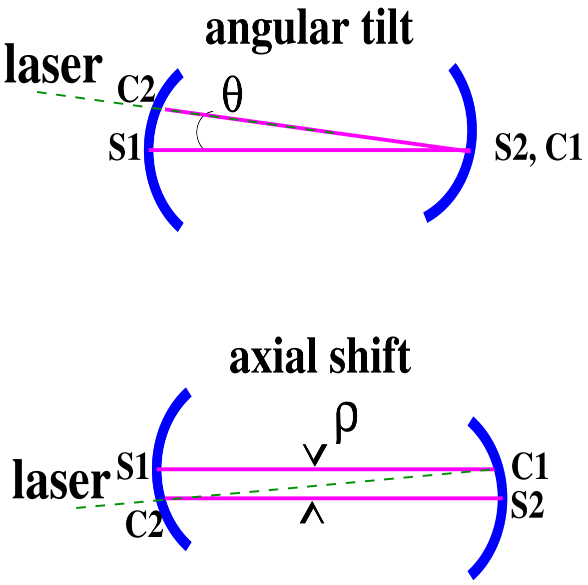

Figure 18: Mechanical defects can be decomposed into two independents effects: angular tilt and axial shift. S1 and S2 are the mechanical mirror centers and C1 and C2 are the mirror optical centers. The laser beam is aligned on the optical axis.

In addition to the length variation – taken into account by the feedback procedure – one has also to consider the effects of mechanical defects. In evaluating these effects we shall

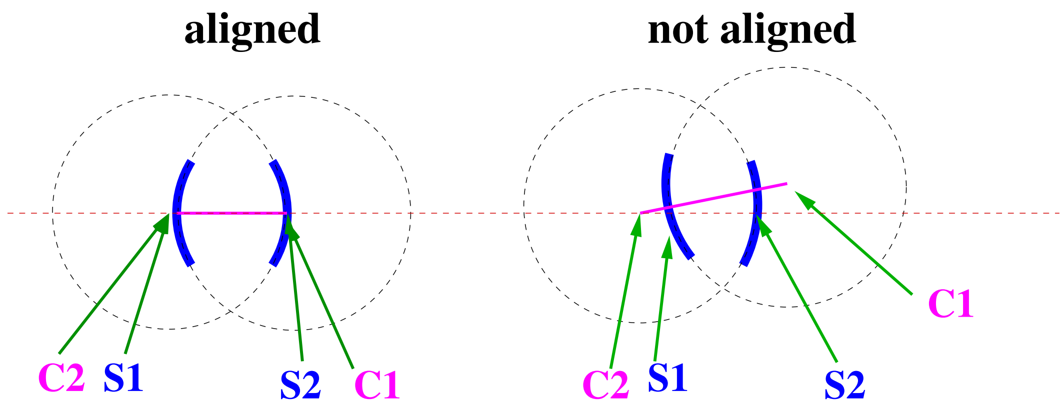

Figure 19: Simple drawing to show the effect of a misalignment of two spherical mirrors.

assume a perfect alignment of the laser beam axis to the cavity optical axis. Power loss due to such a misalignment will be studied in the next section. Two kind of defects are to be considered: an angular tilt θ and a mirror optical axis shift ρ (see fig. 18). In order to understand the effects of such defects on the cavity one can draw a very simple picture (see fig. 19). When the mirror are aligned the optical centers C1 and C2 coincide with the mirror centers S1 and S2. When the mirrors are misaligned, the mechanical axis S1-S2 doesn't coincide anymore with the optical axis C1-C2 of the mirrors. But, since the mirrors are spherical, such misalignments have no effect on the resonance inside the cavity provided the laser beam is aligned with the optical axis. The losses only become significant if the defect is large enough to induce diffraction effects at the mirror edges.

It is very difficult to model the power lost by diffraction inside a Fabry-Perot cavity [12]. However one can estimate it geometrically and thus provide an over estimation of the effect [13, 14]. In ref. [14] the distance D between the optical center C1 and the mirror center S2 is calculated. At first order (= assuming that all defects are small compared to the cavity length) one gets:

$$D \leq \frac{R_c^2}{2R_c - L}\left(\frac{\rho}{R_c} + \theta\right)$$

for the maximum distance induced by an angular tilt of θ radians and an axial shift δ. From this expression one can easily verify that $R_c = L$ (= confocal cavity) minimizes the factor in front of the brackets. Taking $R_c = L = 2$ m, one gets

$$D[mm] = \rho[mm] + 2\theta[mrad]\,.$$

With a 2 m long cavity the order of magnitude of the mechanical tolerances are $O(1mm)$ for the axis shifts and $O(1mrad)$ for the angle tilts.

The usuable radius of the mirror is limited on the one hand by the coating (see A.3), on the other hand by the aperture of the laser tube (see 3.2.3). If R_u is the usuable radius of the mirror, the situation is illustrated in figure 20.

Due to mechanical defects, the optical axis can be shifted on the mirror surface by a distance D from the center. The laser beam width is $\sigma_{spot} \equiv w(z = \pm L/2)/2 = \sqrt{\lambda L/(2\pi)}$. It amounts to ≈ 0.42 mm for $L = 2$ m and for an infrared laser beam. The fractional power loss is calculated according to the following formula:

$$\delta P = \frac{1}{2\pi\sigma_{spot}^2} \int\int_{x^2+y^2>R_u^2} \exp\left(-\frac{(x)^2 + (y-D)^2}{2\sigma_{spot}^2}\right) dxdy$$

where the x and y axes are indicated on the above figure. The results are shown in fig. 21 for $L = 2$ m as function of R_u and for various values of the mechanical tolerance D. Since

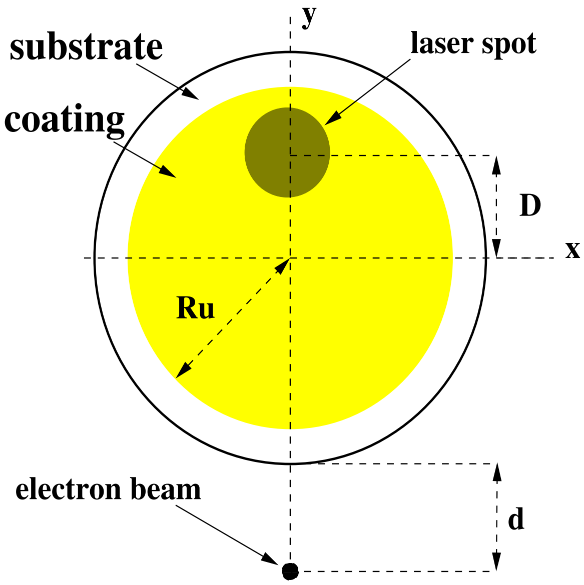

Figure 20: Transverse view of the mirror coating. In this view, d stands for the distance between the electron beam and the lower edge of the mirror.

the coating radius is $\approx$ 12 mm, the aperture from the laser tube, which is at the moment assumed to be 7.5 mm, is defining the usuable area of the mirror. The possible range of offset for the laser beam spot is then around 5 mm.

A.5 Power Losses due to Laser Beam Cavity Coupling Imperfections

As in the above section, there are two independent geometrical misalignments: a shift Δ between the cavity optical axis and the laser axis, an angular α tilt between the laser axis and the cavity axis (see fig. 22). The effect of such defects is to break the axial symmetry inside the cavity. Higher modes (essentially the TEM10 mode, see A.3) are excited and the fundamental Gaussian mode is therefore attenuated. So the power inside the cavity is reduced.

In first order and for small defects the power losses $\Delta P_{in} = P_{0,in} - P_{in}$ ($P_{0,in}$ is the power inside the cavity without any Laser-cavity coupling defects) can be expressed as:

- $\Delta P_{in}/P_{in} = [\alpha\pi w_0/\lambda]^2$ for an angular tilt: if $\alpha \approx 60$ μrad, $\approx 1\%$ of the power is lost.
- $\Delta P_{in}/P_{in} = [\Delta/w_0]^2$ for an axial shift: if $\Delta = 58\mu$m, 1% of the power is lost,

where we have considered a confocal cavity of 2 m length ($w_0 = 582\mu$m).

As mentioned above, resonance is achieved when the laser waist and the cavity waist are matched. Therefore one must also consider the power losses due to these mismatches, too. These defects are shown in fig. 23 (when these defects are present the mode L10 is excited, see A.3). In first order one gets

- $\Delta P_{in}/P_{in} = [\Delta w/w_0]^2$ for a waist size difference of Δw.
- $\Delta P_{in}/P_{in} = [\lambda b/(2\pi w_0^2)]^2$ for a shift of the waist position by a distance b.

The final source of power loss is the laser beam ellipticity (the waist in x and y may be different). Since the optical devices are optimized for one waist value, this means that the axial symmetry is broken in one direction and, again, that higher modes are excited (here

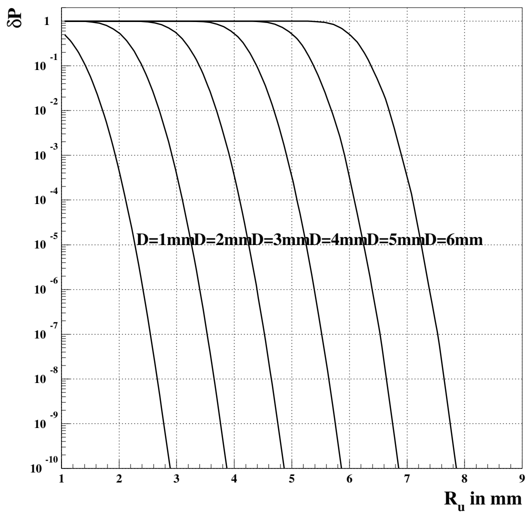

Figure 21: Relative power loss as a function of the usable coating radius for different mechanical defects (see text), for infrared light.

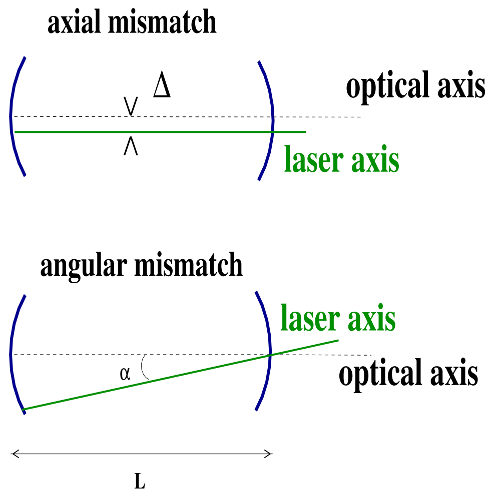

Figure 22: Any laser-cavity coupling geometrical defects can be described by two independent effects: axial mismatch and angular mismatch.

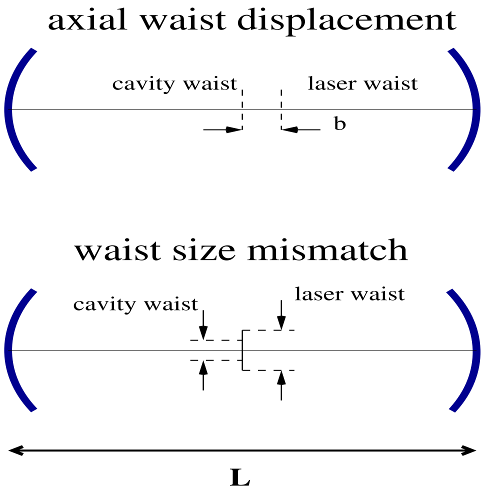

Figure 23: Waist position and size mismatches.

the mode TEM20, see A.3). This effect has been evaluated in [14]. Defining $w_y = \beta w_x$ where w_x and w_y are the laser waists in the two orthogonal directions, the relative power loss is

$$\delta P = \frac{\beta}{1+\beta^2}\left(\frac{\beta^2-1}{\beta^2+1}\right)$$

which amounts to 5% using the numbers given in the LIGHTWAVE laser documentation. This loss is irreducible.

References

[1] POL2000 group: *Proposal for an Upgrade of the HERA Polarimeters for HERA 2000*, DESY-PRC 99-04, and DESY PRC 99-05.

[2] D.P.Barber et.al., *High Spin Polarization at the HERA Electron Storage Ring*, NIM **A 338** (1994) 166.

[3] D.P.Barber et.al., *The First Achievement of Longitudinal Electron Polarization in a High Energy Electron Storage Ring*, Phys. Lett **B 343** (1995) 436.

[4] Hermes Collaboration: *Proposal to DESY for a Longitudinal Electron Polarimeter at the HERA East Section*, September 1994.

[5] R.J. Cashmore et al., *Measurement of Weak Neutral Current Couplings of Quarks at HERA*, in *Future Physics at HERA*, proceedings of the Workshop 1995-96, http://www.desy.de/~heraws96.

[6] F. Zetsche, *Lepton Beam Polarization at HERA*, in *Future Physics at HERA*, proceedings of the Workshop 1995-96, http://www.desy.de/~heraws96.

[7] R. Beyer et al., *Electroweak Precision Tests With Deep Inelastic Scattering at HERA*, in *Future Physics at HERA*, proceedings of the Workshop 1995-96, http://www.desy.de/~heraws96.

[8] S. Levonian, private communication.

[9] See `http://www.cebaf.gov/compton` for a complete documentation.

[10] B. Holzer from the MHE group, private communication.

[11] S. Wipf, private communication

[12] A.E. Siegman, *Lasers*, University Science books, 1986.

[13] J.P. Jorda, *Mise au point d'une cavité Fabry-Perot pour la polarimétrie Compton*, PhD. Thesis, Université Paris 6, 1997. DAPNIA/SPhN-97-04T.
N. Falletto, *Etude, conception er réalisation d'une cavité Fabry-Perot pour le polarimètre Compton de TJNAF*, Université Joseph Fourier-Grenoble 1, 1999. DAPNIA/SPhN-99-03T.

[14] P. Rebougeard, *Note de synthèse sur l'optique de la cavité Fabry-Perot du polarimètre Compton*, Internal note 6112N2000002.
P. Rebougeard, *Tolérance mécanique pour la cavité Fabry-Perot du polarimètre Compton*, Internal note 6112N2000003.

[15] J.M. Mackowski from SMA/IN2P3-Lyon, private communications.

[16] P. Hello, Progress in Optics, Vol. XXXVIII (1998)85-164 and references therein.

[17] P. Hello and J.Y. Vinet, *Analytical models of thermal aberrations in massive mirrors heated by high power laser beams*, J. Phys. France 51 (1990)1267.

[18] P. Hello and J.Y. Vinet, *Analytical models of transient thermoelastic deformations of mirrors heated by high cw laser beams*, J. Phys. France 51 (1990)2243.

[19] Charles Schmit, private communication.